Engineering Science and Technology, an International Journal 47 (2023) 101552

Contents lists available at ScienceDirect

Engineering Science and Technology, an International Journal

journal homepage: www.elsevier.com/locate/jestch

Study the effect of eye diseases on the performance of iris segmentation and recognition using transfer deep learning methods

Abbadullah .H Saleh, Oğuzhan Menemencioğlu *

Karabuk University, Department of Computer Engineering, Karabuk 78050, Turkey

ARTICLE INFO

Keywords:
Iris recognition
Iris segmentation
Eye diseases
Deep learning
Transfer learning
Image processing

ABSTRACT

A new deep learning-based iris recognition system is presented in the current study in the case of eye disease. Current state of art iris segmentation is either based on traditional low accuracy algorithms or heavy-weight deep-based models. In the current study segmentation section, a new iris segmentation method based on illumination correction and a modified circular Hough transform is proposed. The current method also performs a post-processing step to minimize the false positives. Besides, a ground truth of iris images is constructed to evaluate the segmentation accuracy. Many deep learning models (GoogleNet, Inception_ResNet, XceptionNet, EfficientNet, and ResNet50) are applied through the recognition step using the transfer learning approach. In the experiment part, two eye disease-based datasets are used. 684 iris images of individuals with multiple ocular diseases from the Warsaw BioBase V1 and 1,793 iris images from the Warsaw BioBase V2 are also used. The CASIA V3 Interval Iris dataset, which contains 2,639 photographs of healthy iris, is used to train deep models once, and then the transfer learning of this normal-based eye dataset is used to retrain the same deep models using Warsaw BioBase datasets. Different scenarios for training and evaluating participants are used during experiments. The trained models are evaluated using validation accuracy, training time, TPR, FNR, PPR, FDR, and test accuracy. The best accuracies are 98.5% and 97.26%, which are recorded by the ResNet50 (2-layer of transfer learning) model trained on Warsaw BioBase V1 and V2, respectively. Results indicate that the effect of eye diseases is concentrated on the segmentation phase. For recognition, no significant impact is recognized. Some disease that affects the structure (bloody eyes, trauma, iris pigment) can affect the iris recognition step partially. Our study is compared with similar studies in the case of eye diseases. The comparison proves the efficiency and high performance of the proposed methodology against all previous models on the same iris datasets.

1. Introduction

Human biometrics features a subfield called iris recognition that has been widely used in human recognition tasks. Even identical twins' iris patterns differ, and because of the iris' distinctive characteristics, scientists have been able to create incredibly reliable and robust iris identification systems [1,2].

The main problem with human biometrics is their variation over time (such as facial biometrics). Other problems can also cause some issues with human recognition, like exposure to wounds, accidents, burns, and cosmetic surgery (face, fingerprints, palm prints, etc.) [3].

The good news is that the iris is a non-intrusive, high-accuracy biometric. Besides that, previous issues that other biometrics have, are low or do not exist in the iris recognition systems [4,5]. However, many factors affect the iris recognition task, including illumination variations, pose variations, occlusion, and eye diseases [6,7]. Some eye conditions affect both iris segmentation and recognition, whereas in other cases, such diseases have the greatest influence on the iris segmentation phase [6].

There are many eye diseases in which the iris structure can be affected and changed, causing problems for iris recognition systems [8,9]. However, the impact of eye pathology cases on iris segmentation and recognition systems has not been questioned enough.

In the current study, a new iris segmentation method based on modified Hough transform and post-processing techniques to minimize the false positive rate that is common in most recent studies. Another contributing part of the current study is iris recognition in case of disease, which will be studied, and discussed, and all diseases that may

* Corresponding author.
E-mail addresses: abbadullah.h.saleh@gmail.com (A..H Saleh), omenemencioglu@karabuk.edu.tr (O. Menemencioğlu).

https://doi.org/10.1016/j.jestch.2023.101552
Received 31 July 2022; Received in revised form 30 September 2023; Accepted 2 October 2023
Available online 22 October 2023
2215-0986/© 2023 THE AUTHORS. Published by Elsevier BV on behalf of Karabuk University. This is an open access article under the CC BY-NC-ND license (http://creativecommons.org/licenses/by-nc-nd/4.0/).

affect the iris recognition process will be identified. The most recent deep learning models will also be trained using both normal and disease-occurrence-based datasets, and the performance will be evaluated to define the effect of eye diseases on iris recognition part.

In the next section, the related work is presented. Following, the used materials and methods are explained. After that, the results are presented. Finally, the conclusion and future work are illustrated and discussed.

2. Related work

Many studies have been conducted in the iris segmentation and recognition fields. Some of them used the iris image directly, while others applied a segmentation process in the first step.

Roizenblatt et al. [10] proposed an iris recognition system. Their method is applied after cataract surgery. A dataset consisting of 55 eye images related to 55 individuals is used for building the system. In the classification step, the Hamming distance measure is applied. Their results proved that there were six cases in which the recognition failed.

Based on their own gathered dataset, Pierscionek et al. [11] built an iris recognition system. Since the iris ROI was previously obtained, their iris dataset did not require segmentation since it just captured the iris region (not the entire eye). There were only 27 healthy people in the dataset. To normalize the iris, the center of the pupil is also manually found. The study had no evaluation process; it included the iris localization results only.

The case of ocular diseases was discussed in the study of Aslam et al. [12]. Fifty-four individuals with anterior segment diseases were used to build the iris dataset. They built iris templates before and after treatment and used them to apply the iris matching. The Hamming distance measure was used to perform the matching process. The results indicated a degradation in the performance of iris recognition due to the anterior segment diseases (corneal edema, iridotomies, and conjunctivitis).

The IIT Delhi iris database containing 2,240 eyes was used in the research of Minaee and Abdolrashidi [13]. They used the ResNet50 deep learning network and got 95.5 % accuracy.

Trokielewicz et al. [7] were the first to build a disease eye dataset of individuals from the Medical University of Warsaw. Their dataset consisted of 1,288 eye images of 37 individuals, including those with cataract eye disease. The iris recognition part is done using three built-in systems (VeriEye, MIRLIN, and BiomIrisSDK). The researchers compared these iris recognition systems in terms of cataract eye diseases and concluded that the false non-match rate increased compared to the same performance on the normal iris datasets.

Later, they built another dataset called Warsaw BioBase [8]. They used a subset of this dataset, including 1,353 iris images of 219 individuals. Five different categories were used to divide this dataset (Healthy, Tissue, Clear, Geometry, and Obstructions). The common iris recognition systems (MIRLIN, VeriEye, and OSIRIS) were trained using this subset of the Warsaw BioBase dataset. The study used the Failure to Enroll Rate (FTR) to evaluate the performance of these systems. They concluded that the worst performance was related to obstructions and geometry diseases, in which the FTR was 18.36 % and 5.13 %, respectively.

In 2017, they continued their work on the iris and studied the effect of ocular pathologies on the recognition systems. The accumulated dataset of 230 participants consisted of 2,996 eye images and more than 20 eye diseases. The study used four built-in recognition systems (OSIRIS, VeriEye, IriCore and MIRLIN), and considered four concepts. The first one was the influence of eye diseases on the step of enrollment, while the second one was the situation of non-visible changes in the eye structure. The third one was the case in which the eye structure changed, while the final case dealt with the effect on the iris segmentation part. The researchers used a subset of their collected dataset, including 1,353 images of 219 individuals. They proved that the geometrical eye diseases affected the performance significantly by decreasing the FTR. They also concluded that the iris segmentation step was the most influential part of iris recognition systems because of those eye diseases. They also proved that obstructions-related eye diseases affected all steps of the iris recognition system [14].

An effective iris segmentation method was suggested by Rajpal et al. [15]. They proposed the EAI-Net model based on U-Net architecture, treating the segmentation process as a 3-class problem. They also encoded the complex parts of the iris image. A qualitative and quantitative evaluation was applied to evaluate their model using IITD, UBIRISv2, CASIAv4-Interval, and CASIAv4-Thousand datasets.

Sadhya et al. [16] introduced a mechanism for the efficient extraction of consistent bit locations from binarized iris features for biometric systems. Their proposed model formed dynamic clusters of invariant positions from iris feature samples and marked the centers of these clusters as the most consistent locations. They also introduced a criterion called t-consistency for defining the worst-case consistency of IrisCodes with respect to a tolerance threshold. Their model was tested on the *CASIA-V3 Interval* and *CASIAv4 Thousand* databases, achieving 0.88 and 0.65 consistency of the IrisCodes, respectively. However, the proposed model has limitations regarding its efficacy for handling noisy databases.

In a study of Shi et al. [17], an accurate pupil detection and tracking system in a low-quality iris images environment was proposed. The LSTM deep learning architecture was used in the motion detection stage. They trained their models using 10,600 images and 75 videos from three different datasets. They obtained an accuracy of 81 %.

Francese et al. [18] proposed an iris segmentation and localization system in case of Coloboma eye disease. They studied the influence of this disease on the performance of segmentation using two algorithms (Canny edge detector and Daugman's algorithm). The segmentation results showed that 52.63 % and 84.21 % of eye images were incorrectly segmented. In the recognition step, they trained the ResNet50 model using the correctly segmented images (a subset consisting of images taken of 238 individuals) and got a 99.79 % accuracy. Their results needed improvement by enlarging the size of the dataset.

In 2022, a deep iris recognition system in the case of image challenges was proposed by Jia et al. [19]. They used the well-known Convolutional Neural Networks (CNN) and the multi-level interaction methodology to fuse the iris features obtained from multiple CNN models together. They get the benefit of the masking approach to remove the noisy parts of iris images of the CASIA-Iris-V4 thousands, CASIA Iris-V4-Lamp, and ND-IRIS 0405 datasets. To train, validate, and test their system, they accumulated 9,578, 1,092, and 5,321 iris photos. The False Accept Rates (FARs) for the proposed methodologies on CASIA-IrisV4-Thousand, CASIA-IrisV4-Lamp, and ND-IRIS-0405 were 10.41 %, 5.8 %, and 5.49 %, respectively.

Recently, a new challenging iris dataset was collected by Hu et al. [20]. This new dataset was called the CASIA IRIS-Degradation V1 (DV1) dataset, and it includes 3,577 iris images taken from 15 individuals using an acquisition system with no constraints on the imaging conditions. The resultant images included some degradation like occlusion, off-angle large scale, illumination variations, and some glass-existence situations. For both segmentation and recognition steps, researchers used built-in systems. In the segmentation part, they used OSIRIS, IrisSeg, DeepLab, Masek, RTV-L and U-Net. For the recognition part, MaxoutCNN, Masek, OM, UniNet, DGR, and AFINet are used. Results indicated that the U-Net segmentation model was the most precise, with a 95.17 % accuracy, while for the iris recognition part, the best model was UniNet with a 13.13 % Equal Error Rate (EER).

Transfer learning (as a type of deep learning) had been used in many iris recognition systems (for normal and disease-occurrence datasets). Soni et al. combined the NASNet and morphological feature extraction methods to design an iris recognition system based on Circular Hough Transform (CHT). The CASIA dataset was used consisting of 1,344 iris images and obtained a 100 % validation accuracy [21]. The used dataset

Fig. 1. Improved CHT iris segmentation steps (an illustration example).

had no challenge.

The CNN deep network was used in a study by Sujana and Reddy [22]. The CASIA V1 and IITD datasets were used, but only 108 individuals were involved in the experiments. They obtained 95.4 % and 98 % accuracy for the CASIA and IITD datasets, respectively.

Recently, the transfer learning of VGG and MobileNet V2 networks was used in a Ph.D. study [23]. IIT Delhi and MMU2 datasets were used, and a fused dataset containing 1,957 images of 195 individuals was built. Without applying any non-linear scaling, the obtained accuracies of the MobileNet V2 network for the MMU2 dataset were 86 % for the validation set and 90 % for the test set, respectively. However, when non-linear scaling was applied, the accuracies decreased to 86 and 84 %, respectively. Conversely, non-scaling improved the validation accuracy for the IIT Delhi dataset from 82.79 % to 84.774 %. The accuracy was improved by 1.8 % for the test set, which yielded the same outcome. For the VGG network, however, the findings showed that performance was improved when non-linear scaling was used with a factor of 0.8. Although the study provided a few of results in the case of applying non-linear scaling, the experiments still do not show the value of doing so because it performed poorly in several test scenarios.

Some earlier research utilized datasets that were too small, whereas others utilized datasets that had no challenge. In some studies, problems, including variations, eyelid occlusion, noise, iris reflection, etc., were considered. However, there was insufficient research on eye conditions (some concentrated on a specific disease, while others traded with too small dataset size). Among them, some focused only on the impact of eye disorders on iris segmentation, while others investigated the impact of such diseases using well-known built-in systems. The current research is the first to deal with more than 20 eye disease datasets. The research also considers other image degradations like occlusion, illumination variation, and reflection. This study proposes a novel iris segmentation method based on modified circular Hough transform and some post-processing steps to minimize the false positive rate. The research uses the concept of transfer learning to compare many different deep models (ResNet50, GoogleNet, EfficientNet, XceptionNet, Inception_ResNet) and shows the effect of eye diseases on the performance of such models. The study also suggests using two layers of transfer learning and comparing the results. The study will also be compared to the other state-of-art methods in both iris segmentation and recognition to define our contribution.

3. Materials and methodology

3.1. Proposed materials

In this research, two iris datasets are used. The first one is the Warsaw BioBase V1 dataset [9,24], containing 684 iris images taken from 53 individuals, while the second is the Warsaw BioBase V2 dataset [11,12], in which there are 1,793 iris images of 115 individuals. Both datasets include individuals suffering from more than 20 eye diseases, including some natural cases (for one of the left or right eye). Some samples contain one disease, while others may contain multiple ones. Two or three sessions are taken for some individuals in both datasets. The resolution of the images is 640x480, and their format is BMP. Warsaw BioBase V2 includes all the diseases of V1 besides new ones [25]. For the hardware support, a PC with a 64-bit OS, RAM-16.0 GB, an Intel CPU i7-10750H, and a NVIDIA GeForce GTX 1660 Ti with 6 GB of memory are used. On the other hand, for the software support, pertained models (EfficientNet, XceptionNet, Inception_ResNet, ResNet50, and GoogleNet), the image processing toolbox, and the deep learning toolbox of the MATLAB programming environment are used.

3.2. Iris segmentation methodology

There are many known iris segmentation methods that have been used in previous studies. Pupil localization and iris normalization were applied to CASIA Interval-V4 in [26], getting 98 % accuracy. Iris pattern extraction was proposed in [27] to reduce occlusion problems, but this methodology increased the false negative rate significantly. Li et al. [28] suggested using K-means and Residual U-Net for iris semantic segmentation on the CASIA-Iris Thousands dataset. A CNN deep network was used by Trokielewicz et al. [29], getting 3.11 % EER. A Fuzzy-based segmentation model was proposed by Nachar and Inaty [30]. Their experiments on the iris localization step achieved an accuracy of 99.85 %. In the current study, an improved Circular Hough Transform (CHT) segmentation methodology is used based on a previous study [31]. In the first step of this approach, the eye image is pre-processed using an illumination compensation algorithm based on morphological image processing. The pupil is first localized using a threshold, then the morphological opening process is used to illuminate outlier pixels, and the "clear border" operation is applied to remove the unwanted border regions. The radius of the pupil is then computed and used to determine the right border of the iris from which the illumination correction will be applied. The illumination correction strategy adds incremental illumination, starting from the right border of the iris until reaching the right border of the eye image. The same approach is used for the right eye after flipping it so that the operations are still the same for both the left and right eye. As a result, the corrected image will be obtained. In the next step, the original image is closed using a disk structural element to configure a mask image that will be subtracted of the corrected image to remove all illumination variation and get the iris region as a dark part of eye images so that the segmentation will be easier.

For the second step, the CHT is applied and driven using a computed range of iris radius based on the pupil circle, as Eq. (1) shows.

$$\mathrm{Iris}_{\mathrm{Radius}_{\mathrm{range}}} = 2 * \mathrm{MaxL} \pm \mathrm{displacement} \quad (1)$$

Where MaxL is the length of the major axis of the pupil region, and the displacement represents a scalar value that is used to tune the algorithm and obtain the best iris circle (Iris ROI).

In the next step, the iris mask (circle) is obtained. This mask is applied to the original eye image to get the iris circle. The problem with this result is that there will be false positives and false negatives in some cases of occlusion, and this issue is solved by using a post-processing approach in which the high-illumination pixels (representing the non-iris regions) are removed based on a μ-based threshold algorithm (μ represents the mean value of the gray count of the original eye image corresponding to only iris ROI coordinates). Comparing this approach to the previous iris methodology proves that this one removes the non-iris parts and preserves the iris patterns, getting high true positive and true negative rates and low false positive and false negative rates. Fig. 1 illustrates an example of the proposed iris segmentation method where the final iris image has no false positives nor false negatives.

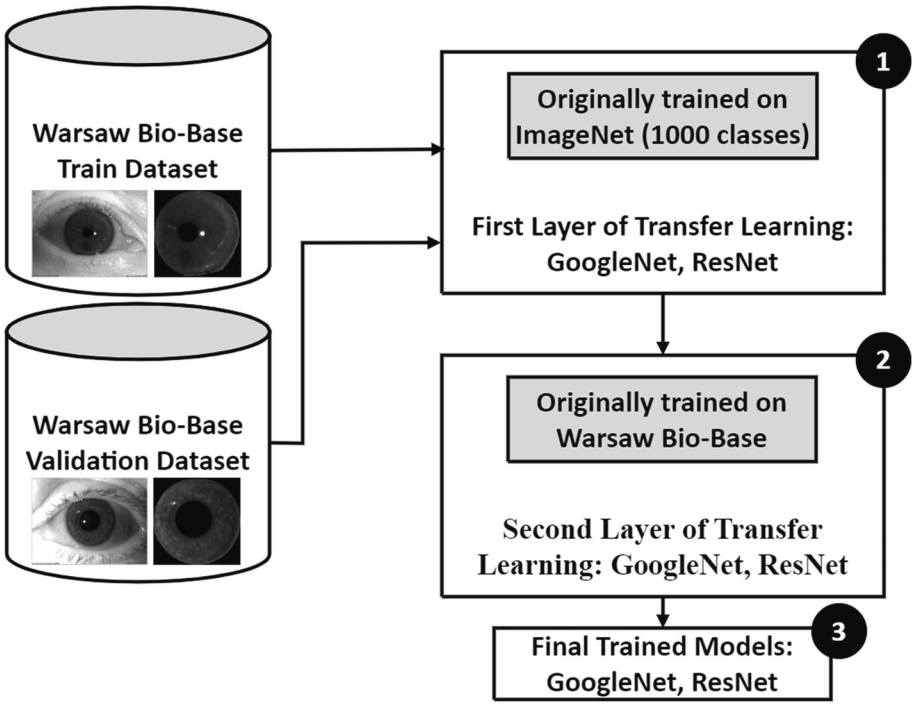

Fig. 2. The proposed transfer learning methodology.

3.3. Iris recognition methodology

Two deep learning models are proposed in this section (ResNet50 and GoogleNet). The transfer learning is used for the learning process to retrain those two models using our iris images rather than their original purpose (image classification), so this will transfer the knowledge of image classification into iris recognition. In terms of machine learning methodologies, transfer learning is often a good solution for knowledge transfer. The process of transferring knowledge from one domain to another is known as transfer learning, and it is considered one of the machine learning strategies [32]. For instance, learning the Turkish language is easier for someone who has previously learned Arabic. The use of transfer learning in recognition applications has been very common.

Iris recognition based on an Alex pre-trained model [33], feature transfer learning for face recognition applications [34,35], and face recognition using GoogleNet [36] are all methods for using transfer learning in different domains.

The transfer learning will be applied once, after that; the trained models will be again used as a second layer of transfer learning, as Fig. 2 illustrates.

3.4. GoogleNet and Resnet50 deep models

Szegedy et al. [37] first suggested GoogleNet, with 22 layers and five pooling layers making up a deep learning convolutional neural network, in the ILSVRC14 competition. This deep network's primary goal was to reduce computation time through effective hardware utilization.

An image measuring 224*224 is what GoogleNet is given as input. The inception layer, where the computations are carried out in parallel, is the main part of this network. Two filters with a combined size of 7*7 constitute the first convolutional layer, which shrinks the input image and retrieves useful data. In the second convolutional layer, the input is decreased by a factor of 4, compared to 8 before the first inception layer. The image size at the first inception layer is 28*28*256, meaning that it is smaller but still has 256 activation maps.

Residual Nets (ResNet50) are a class of deep learning networks with

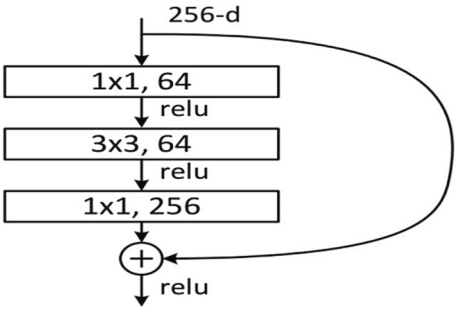

Fig. 3. The Residual Unit.

a depth of 50 layers. The network classifies the 224*224 input image into one of 1000 possible classes. The well-known dataset ImageNet, which contains more than a million photos in a thousand categories, is used to train ResNet. The ResNet has 48 convolutional layers, a max-pooling layer, and an average pooling Fully Connected (FC) layer. This network solves a problem with deep learning called "overfitting," which occurs when the model's depth increases and training error rises. He et al. [38] introduced the new architecture of these networks and called them the residual units, which consist of links that carry out identity connections, seeking two or more convolutional networks to avoid overfitting with deeper layers (Fig. 3) [38].

The MATLAB implementations of GoogleNet [39] and ResNet50 [40] are used in this research. A certain number of classes, different from the original ImageNet classes (1000 classes), will be obtained for each training scenario in our study. The concept is to adjust the network architecture to meet the number of our problem classes. The classification layer and the fully connected (average pooling) layer in each model will be swapped out for new ones. The number of classes in a particular scenario will determine the new size of the FC layer (For instance, if there are 50 people in the iris dataset, the FC layer will be 50x1 in size). The classification layer will be adjusted since the FC layer is being modified to classify the given image into one of the new classes.

Table 1
False Segmentation results of Warsaw BioBase V1.

Person ID	Disease or eye condition	TSR	FSR
0 Left	pseudophakic, glaucoma, condition after acute glaucoma, iridectomy, trabeculectomy, capsulotomy, wide and unresponding pupil	0	6
11 Left	cataract, after acute glaucoma, iridotomy, distorted pupil, posterior synechiae	8	6
12 Left	cataract	5	2
18 Right	retinal detachment (with the silicon oil)		8
20 Left	cataract and corneal haze (at 1 o'clock)	6	1
28 Left	post-trauma cataract, anterior synechiae, iris scarring (at 6 o'clock)	6	1
35 Right	uveitis, secondary glaucoma, cataract, blindness	0	26
39 Left	glaucoma, cataract, condition, iris dialysis, blindness, session 1 and 2: routine examination	0	10
48 Right	rubeosis, synechiae	6	1
53 Right	posterior synechiae	4	4

3.5. Evaluation metrics

The following segmentation metrics are used to evaluate the segmentation process [41]:

True Positives (TP) are the parts of the iris ROI that are correctly classified as iris pixels. True Negatives (TN) are the parts of the non-iris ROI that are correctly classified as non-iris pixels. On the other hand, false negatives and false positives are parts of the iris or non-iris regions that are incorrectly labeled as non-iris or iris pixels.

For the recognition process, the True Positive Rate (TPR), Positive Predictive Rate (PPR), False Negative Rate (FNR), and False Discovery Rate (FDR) are used to evaluate the performance. The TPR represents the ratio of correctly classified samples out of all related true class samples, while the FNR is the opposite concept. PPR represents the ratio of the correctly classified samples out of all predicted class samples, while FDR is the opposite concept.

4. Results and discussion

4.1. The segmentation results

684 cases of Warsaw BioBase v1 and 1,793 cases of Warsaw BioBase V2 datasets are used for the segmentation part. Table 1 and Table 2 include the results of false segmented iris images and their corresponding eye diseases for both Warsaw BioBase V1 and V2 datasets, respectively.

Table 1 and Table 2 show that in most cases, the false segmentation issue occurred due to multiple eye diseases. The eye diseases that have the most influence on the iris segmentation process, are those that change the iris tissues (blindness, retinal detachment, trauma, bloody eyes, synechiae, distorted and dilated pupils). Some of those diseases have temporal effects on iris segmentation, so that the second or third imaging session after treatment makes the iris segmentation possible (i.e., sample "17 Right" contains images taken over two sessions, the results indicate that there are 3 false segmented samples, which are all from session 1 (before surgery)).

For more detailed evaluation, the ground truth of Warsaw BioBase V1 is computed, and the TP, TN, FP, FN, and segmentation accuracy are computed. Fig. 4 includes an illustration of those metrics on a sample of the Warsaw BioBase V1. The red parts are the FPs, while the green parts represent the FNs. The iris region inside the circle represents the TNs, while the rest of the eye image is the FNs. Table 3. includes the average TP, TN, FP, FN, segmentation accuracy, AUC, and EER of Warsaw BioBase V1 & V2. The True Segmentation Rate (TSR) is also computed for both Warsaw BioBase V1 and Warsaw BioBase V2. The TSR is the ratio of the correctly segmented images among all the dataset images.

Table 2
False Segmentation results of Warsaw BioBase V2.

Person ID	Disease or eye condition	TSR	FSR
17 Left	healthy	14	1
17 Right	cataract, pseudophakic	12	3
60 Right	cataract, phacoemulsification with IOL	12	1
62 Right	nuclear cataract, cataract surgery	17	2
63 Left	cataract, posterior synechiae, secondary glaucoma, rubeosis, corneal sweeling and haze, Express implant, trabeculectomy	8	12
65 Left	corneal vascularization, glaucoma, swelling cataract, narrow iris, curled up edges of the iris	0	6
70 Left	retinal detachment, distorted pupil, vitrectomy with oil, aphakia, anterior synechiae	3	1
71 Left	eye trauma and post-traumatic cataract, lens implant with iris diaphragm, iris defect.	3	10
78 Left	eye trauma, aphakia, cornea injury suture, corneal scarring.	5	1
79 Left	intumescent cataract, acute glaucoma condition, aphakia, ECCE.	5	1
81 Right	narrow pupil with symphisis, iris nevus.	4	1
82 Left	glaucoma, pemphigoid, trabeculectomy, pseudophakic, corneal haze, vascularization.	3	4
83 Left	Healthy.	0	7
83 Right	hypermature cataract.	0	5
85 Left	Sweeling, keratopathy, haze in the cornea, iris defect at the top, aphakia.	0	5
7 Right	trabeculectomy, pseudophakic, corneal suture, iridectomies, capsulotomy.	6	1
89 Left	removal of the conjunctiva hypertrophy near the corneal edge, amnion membrane transplantation, cataract	0	6
90 Left	foreign object, corneal injury and sutures, vitrectomy with oil and lens removal, aphakia oil in the anterior chamber.	10	1
92 Left	eye trauma, aphakia, sclera suture, anterior synechiae, severely distorted pupil, corneal scarring.	4	1
93 Right	chemical (gas) burn to the cornea	4	1
95 Left	retinal detachment surgery, blindness, keratopathy, corneal haze	0	5
96 Right	aphakia, retinal detachment surgery, congenital cataract, distorted pupil, anterior synechiae.	4	2
97 Left	trauma, corneal haze	0	6
99 Left	eye trauma, retinal detachment surgery, ECCE, and IOL AC, vitrectomy with oil, corneal transplant with the removal of IOL AC, trabeculectomy, corneal haze, cysts, vascularization.	0	7
100 Right	vitrectomy with oil, blindness, keratopathy, rubeosis, posterior synechiae	0	6
101 Right	glaucoma, cataract	6	0
103 Left	glaucoma, anterior synechiae, ECCE and IOL PC, iris suture.	5	1
104 Left	surgery removal of episcleral cerclage, retinal detachment, cataract, posterior synechiae, distorted pupil.	4	2
106 Right	eye trauma, blood in the anterior chamber, corneal laceration suture.	0	13
107 Left	healthy	4	1
107 Right	retinal detachment, oil in the anterior chamber, aphakia, iridotomy vitrectomy with oil, glaucoma.	4	1
109 Left	healthy	5	1
110 Right	Aphakia, blindness, band keratopathy of the cornea, vitrectomy.	2	4
111 Left	retinal detachment, vitrectomy with oil, pseudophakic, oil in the anterior chamber.	4	1
112 Left	corneal swelling, blood in the anterior chamber, and vascularization	0	6
115 Left	incipient cataract	5	1
115 Right	swelling cataract, ECCE (with prolapse of the vitreous humor into the anterior chamber and bleeding)	0	8
116 Left	ECCE and IOL PC, pseudophakic, capsulotomy	4	2
116 Right	ECCE and IOL PL, pseudophakic, capsulotomy, oval pupil	2	4
1090 Left	uveitis, glaucoma, phacoemulsification with iris correction, aphakia, retinal detachment, fibers	2	5

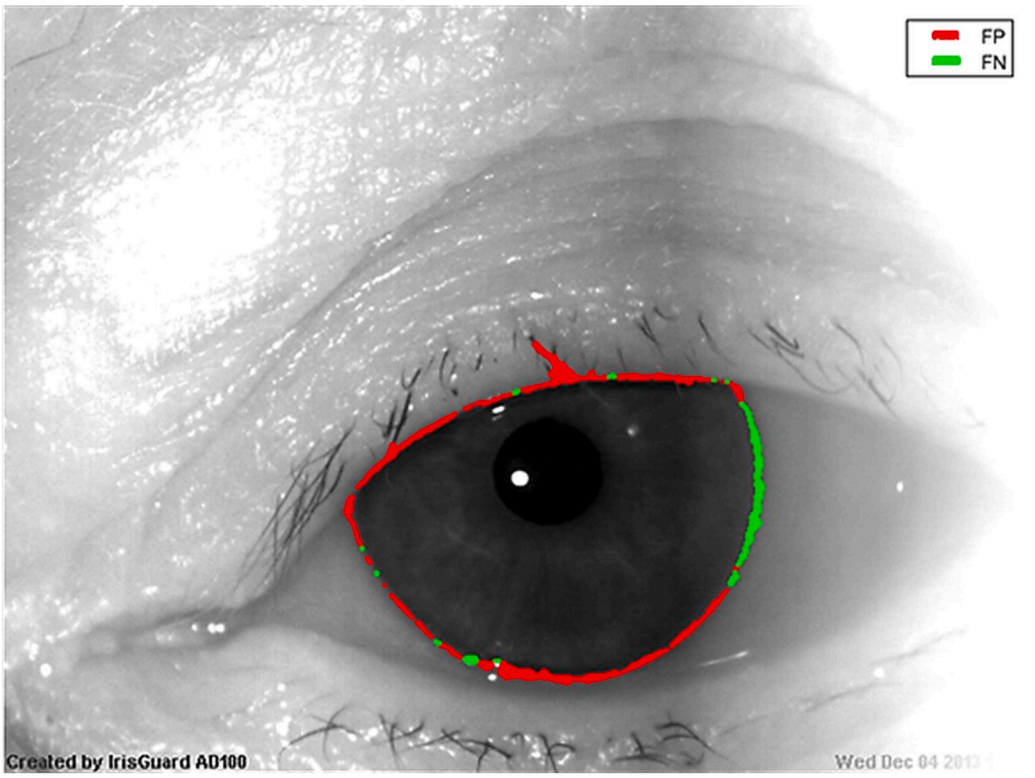

A.

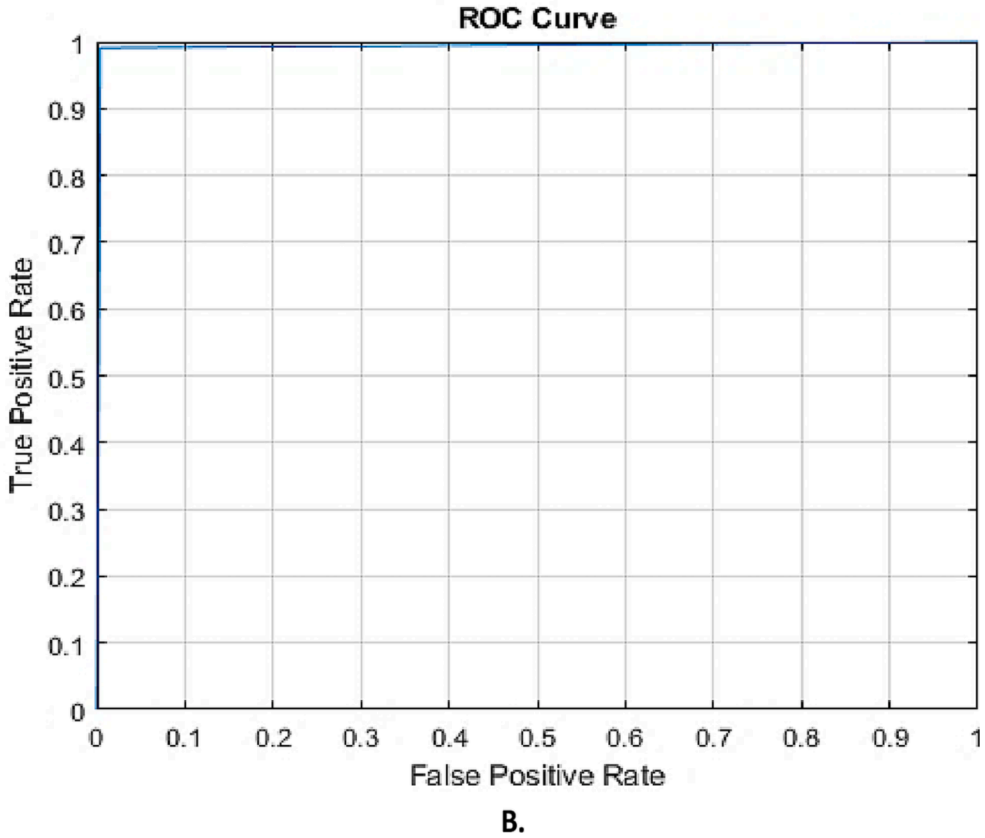

B.

Fig. 4. A. The FP and FN of a segmented sample of Warsaw Bio-Base V1. Dataset, B. The ROC curves of the same sample with AUC = 0.99.

Table 3
Segmentation evaluation metrics of Warsaw BioBase V1 dataset.

Version	TSR %	TPR %	FNR %	TNR %	FPR %	Accuracy %	AUC	EER %
V1	90.5	94.5	5.5	99.2	0.8	98.65	0.975	0.793
V2	87.62	83.5	16.5	97	3	93.5	0.94	3

Table 4
Evaluation results of deep models using Warsaw BioBase V1& V2 datasets.

Metrics/ Models	Warsaw BioBase V1 all samples		Trokielewicz Study [8]	Minaee and Abdolrashidi 2019 [13]	Jia et al. 2022 [19]	Warsaw BioBase V1 Segmented samples		Warsaw BioBase V2 all Samples		Warsaw BioBase V2 Segmented samples	
	ResNet50	GoogleNet	MIRLIN, VeriEye and Biom-IrisSDK	ResNet50	ConvNet with the masking approach	ResNet50	GoogleNet	ResNet50	GoogleNet	ResNet50	GoogleNet
Validation Accuracy (%)	97.1888	90.3614				91.47	78.29	96.3665	90.5213	91.26	80.12
Validation TPR (%)	96.6667	88.8604				91.69	78.49	96.1894	89.7515	90.03	77.01
Validation PPR (%)	98.0121	92.5385				94	80.48	97.1506	92.3009	92.76	86.47
Validation FNR (%)	3.3333	11.1396				8.3	21.5	3.8106	10.2485	9.96	22.98
Validation FDR (%)	1.9879	7.4615				5.9	19.51	2.8494	7.6991	7.32	13.52
Test Accuracy (%)	94.2623	90.9836				96.49	91.22	94.3894	88.7789	90.41	79.45
Test TPR (%)	93.0818	88.9937				96.04	90.19	92.5411	86.0767	89.58	77.23
Test PPR (%)	95.9333	91.6026				97.95	95.28	96.2095	89.9913	94.76	84.78
Test FNR (%)	6.9182	11.0063				3.92	9.8	7.4589	13.9233	10.41	22.76
Test FDR (%)	4.0667	8.3974	8.21–18.36		5.46–10.41	2.04	4.71	3.7905	10.0087	5.23	15.21
AUC	0.978	0.93		0.95		0.98	0.94	0.98	0.92	0.96	0.9
EER	0.05	0.086				0.029	0.069	0.055	0.11	0.07	0.18

4.2. The recognition results

Many training scenarios are performed to evaluate the accuracy of the proposed methodologies. The training scenarios are suggested in different ways. The first scenario (Scenario. 1) studies the effect of eye diseases on both models (GoogleNet, ResNet50) using one layer of transfer learning, while in the second scenario (Scenario. 2), the effect of different splitting criteria (i.e., the percentage of the training, validation, and test set) will be studied.

For the third scenario (Scenario. 3), the two layers of transfer learning will be discussed. For more readability, we will name the four scenarios by their numbers. For scenario. 1, 1,238 grayscale iris images of Warsaw BioBase V1 corresponding with 53 different classes (individuals) are used. For Warsaw BioBase V2, there will be 3,128 iris images of 115 classes. Table 4 includes the detailed results of training and evaluating the deep models using the Warsaw BioBase V1 and Warsaw BioBase V2. The same scenario is performed twice, once for the segmented iris images only and once for the segmented and original iris images (named “all samples” in Table 4). All scenarios are performed using a batch size of 10, the Stochastic Gradient Descent optimizer, and a learning rate of 3e-4. All experiments are done using a data augmentation process, including random reflection, random translation, and random scaling, to improve the training process.

In all cases (validation and test metrics) of Scenario 1, the ResNet50 performance is the best according to validation and test metrics. Using the segmented and original iris images improves the performance

Table 5
Evaluation results of deep models using Warsaw BioBase V1& V2 datasets under different splitting cases.

Metrics/Splitting case	70 % 15 % 15 %		60 % 20 % 20 %		70 % 20 % 10 %	
	ResNet	GoogleNet	ResNet	GoogleNet	ResNet	GoogleNet
Validation Accuracy (%)	90.75	77.31	88.61	76	91.26	80.12
Validation TPR (%)	87.23	76.6	85.14	71.52	90.03	77.01
Validation PPR (%)	93.88	81.11	90.7	82.09	92.76	86.47
Validation FNR (%)	12.76	23.39	14.85	28.47	9.96	22.98
Validation FDR (%)	6.11	18.89	9.29	17.9	7.32	13.52
Test Accuracy (%)	90.41	80.41	87.45	76.23	90.41	79.45
Test TPR (%)	88.24	78.24	84.71	73.89	89.58	77.23
Test PPR (%)	90.08	85.23	91.309	81.7	94.76	84.78
Test FNR (%)	11.75	21.75	15.28	26.1	10.41	22.76
Test FDR (%)	6.91	14.76	8.69	18.29	5.23	15.21

Table 6
Evaluation results of Xception, Inception-ResNet and EfficientNet deep models using Warsaw BioBase V1& V2 datasets using 75%, 15%, 15% training scenario.

Model	Xception	Inception ResNet	EfficientB0
Validation Accuracy (%)	73.1092	86.5546	80.6723
Validation TPR (%)	70.5657	83.6391	78.3639
Validation PPR (%)	77.2765	90.2710	86.5799
Validation FNR (%)	29.4343	16.3609	21.6361
Validation FDR (%)	22.7235	9.7290	13.4201
Test Accuracy (%)	76.6667	81.2500	86.6667
Test TPR (%)	72.7381	79.8065	84.3155
Test PPR (%)	81.7388	84.7756	90.3302
Test FNR (%)	27.2619	20.1935	15.6845
Test FDR (%)	18.2612	15.2244	9.6698

because deep networks work better with more data size. ResNet50 validation accuracy, for example, has increased by 5.7 % and 5.1 % for Warsaw BioBase V1 and V2, respectively. In terms of AUC and EER, The EER values range from around 0.03 to 0.18 where the best cases correspond to ResNet50. Similarly, the AUC of ResNet50 models achieved the best performance.

In Scenario 2, the same iris images of Warsaw BioBase V1 and V2 are used but under different splitting options. Three different splitting cases are used in which the training, validation, and test sets are distributed at different percentages. Table 5 presents a detailed comparison between the GoogleNet and ResNet50 models using different splitting cases.

Scenario 3 aims to transfer knowledge of the learned models after training them on an iris image dataset and reuse them (two-layer training scenario) on the Warsaw versions to improve the models' performance. In the case of segmented iris samples, better recognition accuracy. Since it is well known that GoogleNet and ResNet 50 are trained on large-sized images such as humans, plants, animals, furniture, etc., somehow, these kinds of images are irrelevant to our datasets. To get the maximum benefit of the transfer learning capability, the ResNet50 and GoogleNet models are trained using the well-known CASIA-Interval-V3 dataset [42] (which is a completely healthy iris dataset); meanwhile, the results of the original models and the new transferred ones are compared.

Table 5 proves the fact that the best splitting scenario is 70 % for training, 20 % for validation, and 10 % for testing.

For more investigation of the trained model performance, the experiments of the splitting scenario (75 %, 15 %, 15 %) are repeated using three recent architectures (XceptionNet, EfficientB0 and Inception-ResNet) and shown in Table 6.

Table 6 shows that the best model is the EfficientB0 model with 84.31 % test accuracy.

However, the ResNet50 model has better accuracy than the EfficientB0 model. Comparing the EfficientB0 model with the GoogleNet model shows that the EfficientB0 model has better performance. The only advantage of GoogleNet is that its training time is less than all other models' training time in all experiments, as Fig. 5 illustrates.

Table 7 illustrates the enhancement ratios of training deep models using two layers of transfer learning so that the obtained knowledge of the first trained models will be transferred again to the new models, and the training will be repeated to enhance the performance.

Comparing the original case (one-layer of transfer learning) with the two-layer case proves the fact that using a new layer of transfer learning that is more related to the studied problem (iris recognition) increases the performance significantly. Table 7 shows that the ResNet50 accuracy, for example, is increased by 2 % and 5.9 % for both validation and test sets, respectively, after using the two-layer deep transfer learning on the Warsaw BioBase V1 dataset. Similarly, for Warsaw BioBase V2, the

Table 7
Performance improvement values after using the second layer of transfer learning of Warsaw BioBase V1&V2.

Metrics/Models	Warsaw BioBase V1		Warsaw BioBase V2	
	ResNet50	GoogleNet	ResNet50	GoogleNet
Validation Accuracy (%)	97.41	92.77	93.67	83.43
Validation TPR (%)	97.51	90.54	91.23	81.27
Validation PPR (%)	98.33	93.93	95.87	89.67
Test Accuracy (%)	98.5	94.26	93.15	83.56
Test TPR (%)	98.74	94.02	91.2	83.25
Test PPR (%)	98.42	96.25	95.61	90.4
AUC	0.99	0.98	0.97	0.95

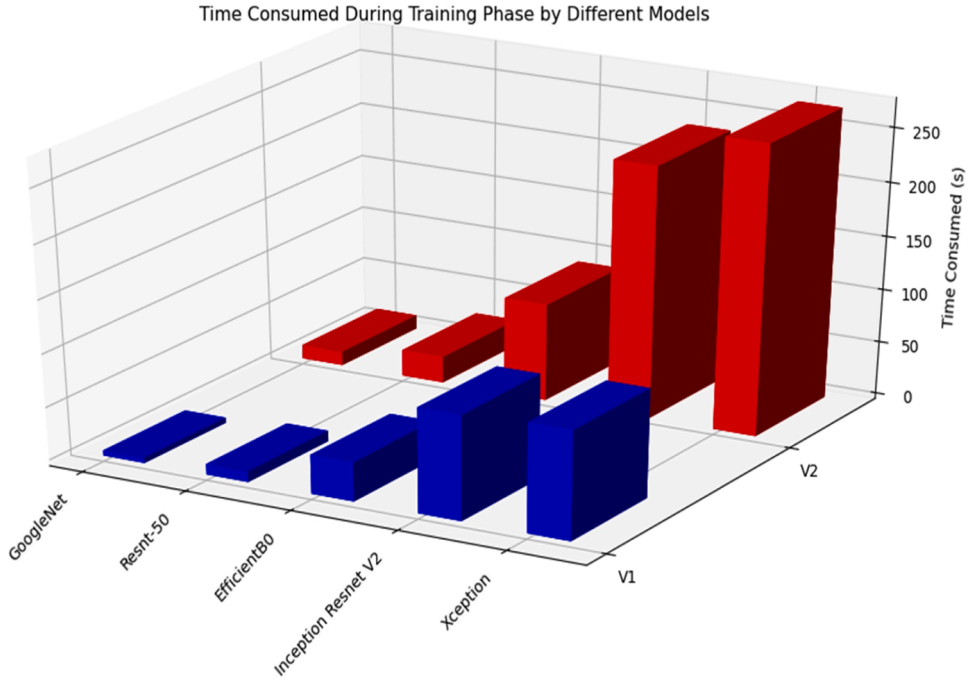

Fig. 5. Time comparative of deep models using Warsaw Bio-Base V1&V2.

Table 8
Different epochs effects on training 2-layers transfer learning of ResNet50 on Warsaw BioBase V2 dataset.

Epochs/Metrics	20	50	100	300	400	500
Validation Accuracy	93.67	94.87	92.77	94.27	95.78	94.57
Validation TPR (%)	91.23	92.05	90.85	92.54	94.8	91.24
Validation PPR (%)	95.87	96.08	94.48	95.76	95.72	95.95
Test Accuracy (%)	93.15	90.4	97.26	95.2	95.2	96.57
Test TPR (%)	91.2	89.27	97.22	94.12	95.06	95.83
Test PPR (%)	95.61	95.19	97.97	97.05	96.5	98.2

validation and test accuracy are increased by 2.74 % and 2.4 %, respectively. All other metrics (TPR, PPR, FNR, and FDR) are also improved.

For deeper results, we repeated the experiments using a different number of epochs to reach the best performance. In Table 8, the results of training models with epochs from 20 to 500 are shown. Table 8 proves that the bestResNet50 performance corresponds to the 500 epochs training case. To know the most influential diseases on the iris recognition system, the performance results are used to identify samples with the highest error rates and less accuracy. Table 9 includes the most frequent fault samples of the GoogleNet and ResNet50 models trained by Warsaw BioBase V2. Table 9 demonstrates that with more eye diseases, GoogleNet's performance degrades. Though, this conclusion is not applicable to ResNets, which are not impacted by eye diseases like GoogleNet. The "0090" and "0060" samples are the only frequently-fault samples in GoogleNet and ResNet. Sample "0090" contains two false discovery errors in ResNet50 and one false negative error in GoogleNet. On the other hand, sample "0060" for GoogleNet has one false negative and two false discovery mistakes. However, when the number of ResNet model epochs increased, the bulk of these frequent errors vanished. For the EfficientNet model, there are two frequent fault samples ("0016L" and "0064L") that contain multiple diseases (glaucoma, cataract, iridotomy, posterior synechia, bloody eyes, iris pigment), causing big changes in eye's tissues. Eye disease has less of an impact on iris recognition than it does on iris segmentation. Some cases of eye blindness are easily recognized. The eye condition in which the iris is covered, or its structure is altered completely or partially has the most significant impact on iris recognition. To show the importance of the current research, Table 10 includes a detailed comparative study between the

Table 9
Frequent faults of training GoogleNet, ResNet50, and EfficientNet using Warsaw BioBase V2 dataset.

GoogleNet				ResNet50				EfficientNet			
Class	Sumr	Sumc	TP	Class	Sumr	Sumc	TP	Class	Sumr	Sumc	TP
0004L	1	2	1	0011L	2	1	1	0016L	6	10	5
0005L	2	1	1	0028L	1	1	0	0024L	2	4	2
0017L	3	4	2	0031L	1	1	0	0030L	2	4	2
0021L	1	2	1	0076L	1	2	1	0042L	2	4	2
0022L	1	3	1	0090L	2	4	2	0064L	5	6	3
0023L	1	2	1	1090L	1	2	1	1090L	1	1	0
0031L	1	2	1								
0039L	1	2	1								
0060L	2	3	1								
0063L	3	1	1								
0064L	4	8	4								
0071L	2	1	1								
0090L	2	1	1								
1111L	1	2	0								

Table 10
Comparative of the present study and relevant literature.

Authors	method	Dataset/No. Of Images	Dataset Challenge	Performance/Observations
Current Research	GoogleNet, ResNet50	Warsaw BioBase V1/684 Images, Warsaw BioBase V2 1793 Images. CASIA-V3.0/ 2639 Images.	Eye disorders include wide noise factors such as Images with different sessions, before and after treatment, illumination conditions, Occlusion, eyelids and eyelashes noise, and high dilated pupils.	For Warsaw BioBase V1: ResNet50 ACC = 98.5 %, GoogleNet ACC = 94.26 % For Warsaw BioBase V1: ResNet50 ROC (AUC) = 0.99, GoogleNet ROC (AUC) = 0.98 For Warsaw BioBase V2: ResNet50 = 97.26 %, GoogleNet = 93.15 % For Warsaw BioBase V2: ResNet50 ROC (AUC) = 0.97, GoogleNet ROC (AUC) = 0.95 Segmentation: EER (V1) = 0.793 %, EER(V2) = 3 %.
Trokielewicz et al. 2015 [8]	MIRLIN, VeriEye and Biom-IrisSDK	Warsaw BioBase V2/included 1353 images of 219 individuals.	Eye disorders	Obstructions of MIRLIN (FTR) = 18.36 % Obstructions of OSIRIS (FTR) = 8.21 % Geometry of VeriEye (FTR) = 5.13 %. The low performance is attributed to segmentation errors.
Roizenblatt et al. 2004 [10]	Hamming distance	55 images of different eyes	Cataract (surgery challenges)	There were six cases of unsuccessful recognition.
Minaee and Abdolrashidi 2019 [13]	ResNet50 (Pretrained model)	The Indian Institute of Technology in Delhi/2,240 Iris Images of 224 Individuals.	Some samples differed in size and color distribution, but no challenges were mentioned.	ACC = 95.5 %, They utilized the raw images without segmentation step but a saliency map to recognize the iris ROI used. Additionally, few samples were used for testing.
Trokielewicz et al. 2017 [14]	MIRLIN, OSIRIS, VeriEye and IriCore	1353 photos of 219 individuals and excluded eleven distinct irises.	Eye disorders	Ocular obstruction diseases cause the majority of iris recognition deterioration. Due to the segmentation faults, performance decreases.
Jia et al. 2022 [19]	ConvNet with the masking approach	ND-IRIS 0405, CASIA IrisV4-Lamp, and CASIA-IrisV4 Thousand.	Noise (Iris recognition in less restrictive environments)	CASIA Thousand (FAR) = 10.41 %. CASIA Lamp (FAR) = 5.8 %. ND-IRIS-0405 (FAR) = 5.49 %.

current study and other previous ones.

Where the Sumr represents the total number of true and wrong samples across the horizontal axis, Sumc: the total number of true and wrong samples along the vertical axis, TP: true positives (The frequent false detected samples are emphasized.).

5. Conclusion

Concerning ocular diseases, a new iris recognition system based on deep learning is presented. Two various deep learning models (ResNet50 and GoogleNet) are used for the recognition phase using the transfer learning methodology. Two different datasets are used in the experiments. The Warsaw BioBase V1 dataset, which includes 684 images of iris with various eye diseases, is the first dataset. The second dataset is the Warsaw BioBase V2, which includes 1,793 iris images with more complicated eye diseases and a higher number of images. The Warsaw BioBase V1 and V2 image acquisition processes consider two or three sessions.

Various training scenarios are used to apply experiments. Different deep learning models, various splitting criteria, and transfer learning are all considered in the suggested scenarios. Many evaluation metrics are used to assess the performance of the result models, including TPR, FNR, PPR, FDR, training accuracy, training time, validation accuracy, test accuracy, AUC, and EER. Besides that, an analysis of how eye conditions impact the performance of iris segmentation and recognition is introduced and discussed. Results showed that eye diseases could sometimes significantly impact iris segmentation, especially in situations with a combination of diseases, pupil issues, some retinal detachments, blindness, and bloodshot eyes. The results also show that most eye conditions, like glaucoma, cataracts, blurry vision, and some lens and corneal problems, do not affect iris segmentation when they exist separately.

The most significant influence on iris recognition comes from eye conditions where the iris is entirely or partly covered, or its structure is altered. In addition, the results confirm that most of the special-eye cases can be accommodated by iris recognition systems with no major issues. The results also show that some eye conditions may reduce the ability to recognize the iris and must be ruled out or treated before being used in biometric systems.

Declaration of Competing Interest

The authors declare that they have no known competing financial interests or personal relationships that could have appeared to influence the work reported in this paper.

Acknowledgments

This paper summarizes a portion of Abbadullah .H SALEH M.Sc. thesis research at Karabuk University in 2022, supervised by Dr. Oğuzhan Menemencioğlu.

References

[1] V. Kakkad, M. Patel, M. Shah, Biometric authentication and image encryption for image security in cloud framework, Multiscale and Multidisciplinary Modeling, Experiments and Design 2 (4) (2019) 233–248.
[2] J.G. Ravin, Iris Recognition Technology (or, Musings While Going through Airport Security), Ophthalmology 123 (10) (2016) 2054–2055.
[3] S. Rajarajan, S. Palanivel, K.R. Sekar, S. Arunkumar, Study on the diseases and deformities causing false rejections for fingerprint authentication, Int. J. Pure Appl. Math. 119 (15) (2018) 443–453.
[4] Y. Moses, Y. Adini, S. Ullman, "Face recognition: The problem of compensating for changes in illumination direction", Lecture Notes In Computer Science (Including Subseries Lecture Notes In Artificial Intelligence And Lecture Notes In Bioinformatics), 800 LNCS (7): 286–296 (1994).
[5] X. Xie, K.-M. Lam, Face recognition under varying illumination based on a 2D face shape model, Pattern Recogn. 38 (2) (2005) 221–230.
[6] F. Alonso-Fernandez, J. Bigun, Quality factors affecting iris segmentation and matching. Proceedings - 2013 International Conference On Biometrics, ICB 2013, 2013.
[7] M. Trokielewicz, A. Czajka, P. Maciejewicz, Cataract influence on iris recognition performance, Photonics Applications In Astronomy, Communications, Industry, And High-Energy Physics Experiments 9290 (2014), 929020.
[8] M. Trokielewicz, A. Czajka, P. Maciejewicz, Assessment of iris recognition reliability for eyes affected by ocular pathologies. 2015 IEEE 7th International Conference On Biometrics Theory, Applications And Systems, BTAS 2015, 2015.
[9] M. Trokielewicz, A. Czajka, P. Maciejewicz, Database of iris images acquired in the presence of ocular pathologies and assessment of iris recognition reliability for disease-affected eyes, in: Proceedings - 2015 IEEE 2nd International Conference On Cybernetics, CYBCONF 2015, 2015, pp. 495–500.
[10] R. Roizenblatt, P. Schor, F. Dante, J. Roizenblatt, R. Belfort, Iris recognition as a biometric method after cataract surgery, Biomed. Eng. Online 3 (2004) 1–7.
[11] B. Pierscionek, S. Crawford, B. Scotney, Iris recognition and ocular biometrics-the salient features, in: Proceedings - IMVIP 2008, 2008 International Machine Vision And Image Processing Conference, 2008, pp. 170–175.
[12] T.M. Aslam, Z.T. Shi, B. Dhillon, Iris recognition in the presence of ocular disease, J. R. Soc. Interface 6 (34) (2009) 489–493.
[13] S. Minaee, A. Abdolrashidi, DeepIris: Iris Recognition Using A Deep Learning Approach, arXiv:1907.09380v1 (2019).
[14] M. Trokielewicz, A. Czajka, P. Maciejewicz, Implications of ocular pathologies for iris recognition reliability, Image Vis. Comput. 58 (2017) 158–167.
[15] S. Rajpal, D. Sadhya, K. De, P.P. Roy, B. Raman, Eai-net: Effective and accurate iris segmentation network, in: Pattern Recognition and Machine Intelligence: 8th International Conference, PReMI 2019, Tezpur, India, December 17-20, 2019, Proceedings, Part I, Springer International Publishing, 2019, pp. 442–451.
[16] D. Sadhya, K. De, B. Raman, P.P. Roy, Efficient extraction of consistent bit locations from binarized iris features, Expert Syst. Appl. 140 (2020) 112884.
[17] L. Shi, C. Wang, F. Tian, H. Jia, An integrated neural network model for pupil detection and tracking, Soft. Comput. 25 (15) (2021) 10117–10127.
[18] R. Francese, M. Frasca, M. Risi, Are IoBT services accessible to everyone? Pattern Recogn. Lett. 147 (2021) 71–77.
[19] L. Jia, X. Shi, Q. Sun, X. Tang, P. Li, Second-order convolutional networks for iris recognition, Appl. Intell. 52 (10) (2022) 11273–11287.
[20] J. Hu, L. Wang, Z. Luo, Y. Wang, Z. Sun, A Large-scale Database for Less Cooperative Iris Recognition, in: 2021 IEEE International Joint Conference On Biometrics, IJCB 2021, 2021, pp. 1–6.
[21] A. Soni, T. Patidar, M.R. Kumar, K.P. Bharath, S. Balaji, R. Rajendran, Iris Recognition using Hough Transform and Neural Architecture Search Network, in: 3rd IEEE International Virtual Conference On Innovations In Power And Advanced Computing Technologies, I-PACT 2021, 2021, pp. 1–5.
[22] K. Devi, An effective feature extraction approach for iris recognition system, Indian J. Sci. Technol. 9 (1) (2016) 1–5.
[23] C. Science, K.B. Shah, On human iris recognition for biometric identification based on various convolution neural networks, Gujarat Technological University, 2022.
[24] *Biometrics and Machine Learning Group, Warsaw-Bio-Base-Disease-Iris v1.0, Warsaw University of Technology, (2015).*
[25] *Biometrics and Machine Learning Group, Warsaw-Bio-Base-Disease-Iris v2.1, Warsaw University of Technology, (2015).*
[26] A.M. Mayya, M.M. Saii, Iris recognition based on weighting selection and fusion fuzzy model of iris features to improve recognition rate, Int, J. Inform. Res. Rev. 03 (2016) 2664–2680.
[27] S.A. Naji, R. Tornai, J.H. Lafta, H.L. Hussein, Iris recognition using localized zernike features with partial iris pattern, Commun. Computer Inform. Sci. 1183 CCIS (2020) 219–232.
[28] Y.H. Li, W.R. Putri, M.S. Aslam, C.C. Chang, Robust iris segmentation algorithm in non-cooperative environments using interleaved residual u-net, Sensors 21 (4) (2021) 1–21.
[29] M. Trokielewicz, A. Czajka, P. Maciejewicz, Post-mortem iris recognition with deep-learning-based image segmentation, Image Vis. Comput. 94 (2020), 103866.
[30] R. Nachar, E. Inaty, An effective segmentation method for iris recognition based on fuzzy logic using visible feature points, Multimed. Tools Appl. 81 (7) (2022) 9803–9828.
[31] Saleh H. Abbadullah, O. Menemencioğlu, A dynamic circular hough transform based iris segmentation, in: Emerging Trends in Intelligent Systems & Network Security, Springer International Publishing, Cham, 2022, pp. 9–20.
[32] F. Zhuang, Z. Qi, K. Duan, D. Xi, Y. Zhu, H. Zhu, H. Xiong, Q. He, A Comprehensive Survey on Transfer Learning, Proc. IEEE 109 (1) (2021) 43–76.
[33] M.A. Nirgude, S.R. Gengaje, Iris Recognition System Based on Convolutional Neural Network, Springer, Singapore, 2022.
[34] X. Yin, X. Yu, K. Sohn, X. Liu, M. Chandraker, Feature transfer learning for face recognition with under-represented data, in: Proceedings Of The IEEE Computer Society Conference On Computer Vision And Pattern Recognition, 2019, pp. 5697–5706.
[35] C.X. Ren, D.Q. Dai, K.K. Huang, Z.R. Lai, Transfer learning of structured representation for face recognition, IEEE Trans. Image Process. 23 (12) (2014) 5440–5454.
[36] K.O. Mohammed Aarif, S. Poruran, OCR-Nets: Variants of Pre-trained CNN for Urdu Handwritten Character Recognition via Transfer Learning, Procedia Comput. Sci. 171 (2019) (2020) 2294–2301.
[37] C. Szegedy, W. Liu, Y. Jia, P. Sermanet, S. Reed, D. Anguelov, D. Erhan, V. Vanhoucke, A. Rabinovich, Going Deeper With Convolutions, in: Proceedings Of The IEEE Conference On Computer Vision And Pattern Recognition, Boston, Massachusetts, 2015, pp. 1–9.
[38] K. He, X. Zhang, S. Ren, J. Sun, Deep residual learning for image recognition, in: Proceedings Of The IEEE Conference On Computer Vision And Pattern Recognition, Las Vegas, NV, USA, 2016, pp. 770–778.

[39] Internet: Mathworks.com, “”googlenet.Html,“ Mathworks”, available: https://www.mathworks.com/help/nnet/ref/googlenet.html. . (2021).
[40] Internet: Mathwork.com, “”resnet50,“ Mathwork”, available: https://www.mathworks.com/help/deeplearning/ref/resnet50.html;jsessionid=0997fbde6e724213cdf6a294bfa4. (2021).
[41] Internet: Mathwork, “Mathwork, Assess Classifier Performance Mathwork 2020 [Online].”, available: https://www.mathworks.com/help/stats/assess-classifier-performance.html.
[42] “CASIA-IrisV3 Interval, Chinese Academy of Science. http://www.cbsr.ia.ac.cn/english/IrisDatabase.asp. [Accessed 1 12 2020]”.